Article

Cooling Performance Prediction for Hydraulic Thermoelectric Radiant Cooling Panels with Experimental Validation

Minseong Kim [ID]**, Yong-Kwon Kang, Jaewon Joung and Jae-Weon Jeong *** [ID]

Department of Architectural Engineering, College of Engineering, Hanyang University, 222 Wangsimni-Ro, Seongdong-Gu, Seoul 04763, Republic of Korea
* Correspondence: jjwarc@hanyang.ac.kr; Tel.: +82-2-2220-2370

Abstract: Thermoelectric technology has been developed as a substitute for existing refrigerants in heating, ventilation, and air-conditioning system applications for building decarbonization. A hydraulic thermoelectric radiant cooling panel (hTERCP) operated based on the Peltier effect can alternate a conventional cooling system using a chiller with refrigerators. This study aimed to develop a cooling performance prediction model for a hTERCP-integrated free cooling system according to the desirable range of five design factors. A mockup model of the hTERCP was constructed and tested in an environmental chamber to verify the proposed simulation model. The simulation and the experimental analysis confirmed that the heat rejection performance of the thermoelectric module (TEM) significantly affects the cooling performance of the hTERCP. The cooling water temperature was the primary design factor for releasing heat from the hot side of the TEM and significantly influenced the cooling performance of the hTERCP. A parametric analysis of the five design factors was conducted to investigate a method for improving the coefficient of performance (COP) of the hTERCP. The cooling water temperature affected the COP by 38.6–45.7%, and the heat exchange area of the cooling surface greatly influenced the cooling performance by 41.4%. The cooling water flow rate, heat exchange effectiveness of the water block, and heat resistance of the hot side were confirmed to have relatively little influence as 9.7–10.2%, 11.9–24.8%, and 0.7–11.1%, respectively.

Keywords: thermoelectric module; radiant cooling panel; cooling performance prediction model; design factor; parametric analysis; impact analysis

1. Introduction

Thermoelectric modules (TEM) have attracted substantial attention as non-vapor compression refrigeration technologies to prevent global climate changes and ozone layer depletion [1–4]. Their advantages include fast response, compact size, no noise, no vibration, and no moving parts without a refrigerant that can be used for heating, ventilation, air-conditioning, and refrigeration (HVAC&R) [5–9]. TEM has been studied as a solid-state heat pump based on the Peltier effect since the early 2000s [10]. Thermoelectric radiant cooling panel (TERCP)-installed TEMs were recently proposed and developed as alternative radiant cooling systems to conventional radiant cooling panels using chilled water [11]. Although the TEM has a relatively low coefficient of performance (COP) compared to the vapor compression cooling system, it is expected to be a renewable and sustainable energy source in building air-conditioning systems [12–15].

The TEM has been proposed as an air heating and cooling system in an HVAC system. Irshad et al. [16] suggested a design method for determining the photovoltaic wall-integrated thermoelectric air-cooling duct size. The energy consumption and amount of CO_2 generated were experimentally evaluated. The proposed system could reduce 60.2 tons of CO_2 compared with the conventional air-cooling system, which would pay back in 4.8 years. Cheon et al. [17] proposed the thermoelectric heat pump (TEHP) with a dedicated outdoor air system (DOAS). The TEHP was used as an air-to-air heat pump to

recover the waste heat from the returned air from the conditioned zone. A performance prediction model of the TEHP was developed by the experiment, and an energy simulation was conducted annually to derive the energy-saving potential of the TEHP. The results showed that the energy-saving point of the heat sink was 0.49 of the heat exchange effectiveness for heat recovery.

Furthermore, a TEM was used as the radiant cooling system. Lertsatitthanakorn et al. [18,19] derived the thermal comfort and the heating and cooling performances of a water-cooled thermoelectric panel (TERP). Lim et al. [20] investigated the annual energy consumption of a TERP and its energy-saving potential while using a DOAS. Luo et al. [21] suggested an air-cooled TERP with a building-integrated photovoltaic (TEBIPV) system and developed numerical models via simulation. The performance of the TEBIPV wall was numerically analyzed. The results illustrated that the energy-saving rate of the TEBIPV was approximately 480% in several cities in China. Shen et al. [22,23] proposed a method for using an air-cooled TERP with numerical models to estimate the developed designs. Lim et al. [24,25] developed an empirical model and a numerical design tool to predict the cooling performance of an air-cooled TERP.

Although the air-cooled TERP has been studied and researched for several years, there are still limits to improving the energy efficiency of the air-cooled type due to the performance limitations of the TEM. Moreover, there are few guidelines and no standard models of water-cooled TERCPs for application in building energy simulation and performance evaluation. Therefore, the primary objective of this study was to develop a cooling performance prediction model for a hydraulic thermoelectric radiant cooling panel (hTERCP)-integrated free cooling system according to the desirable range of design factors. The simulations and experiments were conducted based on previous studies to derive the valid cooling performance of the hTERCP [26,27]. Based on the analyzed and measured data, the analysis of variance (ANOVA) method was used to develop an energy prediction model, which was verified by an additional experiment. Finally, the basic guidelines of an hTERCP are presented for use in HVAC design in building energy simulations.

2. System Overview

As shown in Figure 1, when electricity is input to the TEM, a temperature difference occurs on both surfaces of the TEM. This is called the Peltier effect, and the cold side of the TEM is used as the cooling source for the hTERCP. The hTERCP consists of TEMs, water blocks, water pipes, aluminum panels, and insulation, as shown in Figure 2. The TEMs were installed on an aluminum panel to absorb the heat from its surface to the water blocks using TEMs with the Peltier effect. To prevent the degradation of the cooling performance by undesirable heat transfer, the insulation adheres to the top side of the aluminum panel, water blocks, and water pipelines.
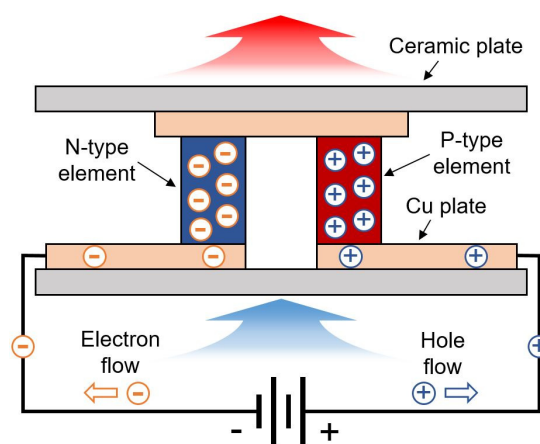
Figure 1. Principle of Peltier effect at the TEM.
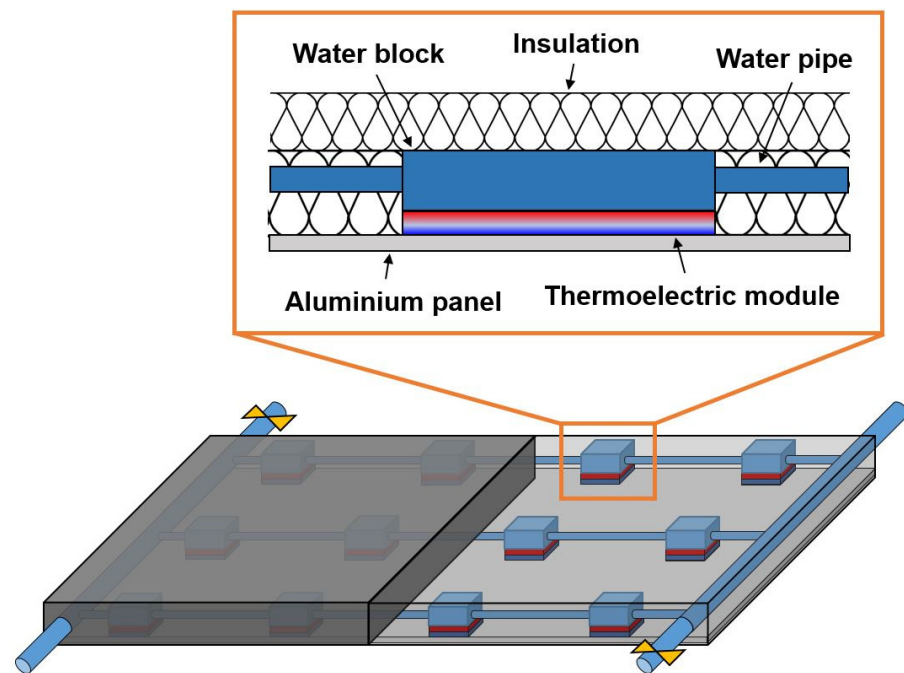
Figure 2. Configuration of hTERCP.

The hTERCP was set up as a ceiling panel in the conditioned zone to remove the sensible cooling load by radiative and convective heat transfer while maintaining the surface temperature of the panel. Therefore, the latent cooling load should be removed by a primary ventilation unit, such as a DOAS, before the operation of the hTERCP, as shown in Figure 3. According to the ASHRAE guidelines [28], it is generally recommended that the surface temperature of the radiant cooling panel should be 0.5 °C higher than the dew point temperature of the conditioned zone to prevent condensation. Likewise, the temperature difference between the hottest and coldest spots of the cooling surface should be within 3 °C to ensure the uniformity of the cooling panel.

Figure 3. Schematic diagram of the hTERCP with DOAS in the conditioned zone.

The radiative heat transfer was calculated using the absorption factor of the panel surface and the mean radiant temperature (MRT) of the conditioned zone. The absorption factor can be enhanced by painting a color with high absorptivity based on material properties. The ceiling, floor, and walls of the environmental chamber where th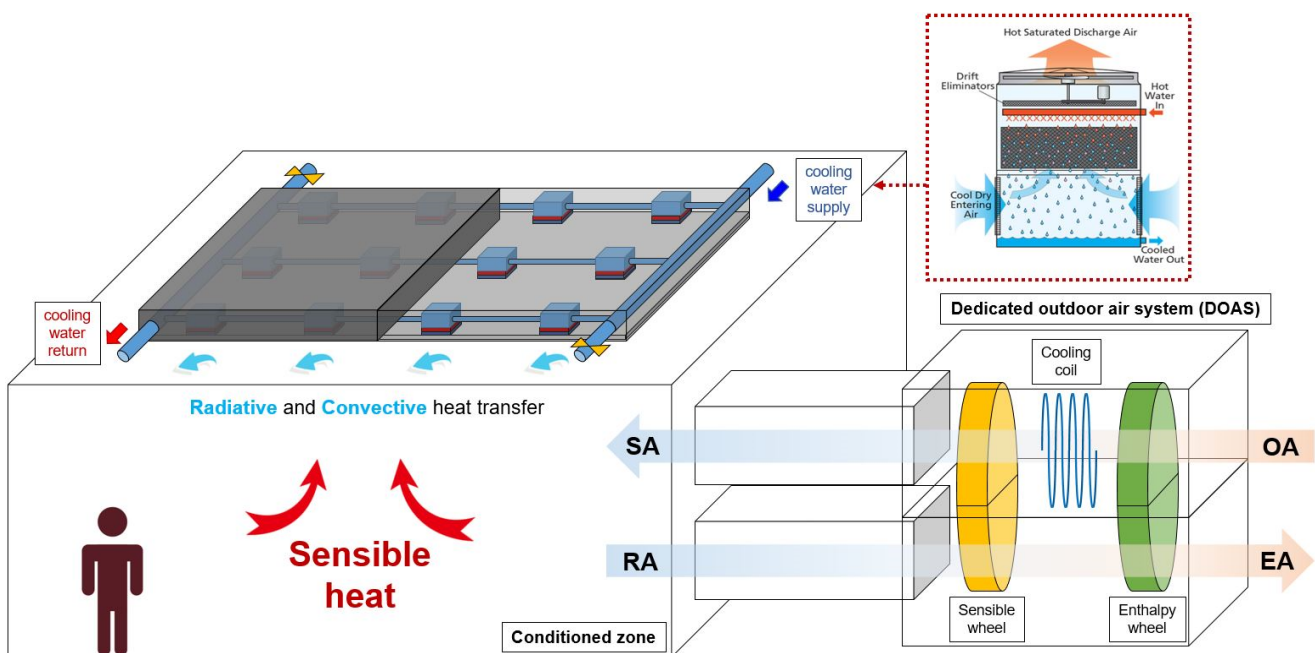e hTERCP was installed on the top side were insulated to stabilize the surface temperature because the MRT is dependent on the surface temperature of the room.

3. Simulation Model Analysis

3.1. Model Parameters

As shown in Table 1, five design factors were selected based on previous studies. The temperature of the cooling water supply (T_{cws}) ranged from 24 to 28 °C, which can be produced from a cooling tower without a chiller operation in Korean weather [29]. The flow rate of the cooling water supply ($\dot{m}_w$) was classified as laminar or fully turbulent according to the shape of the hydraulic cooling system. The heat exchange effectiveness of the water blocks (ε_{WB}) for the simulation model was calculated using Equation (1). The maximum heat exchange effectiveness was assumed to depend on the commercial heat exchanger. The cooling surface heat exchange area (A_c) can be extended by up to 41% with a corrugated shape to avoid facing each other. The minimum and maximum thermal resistances of the hot side (R_h) were investigated in a previous study [30]. Table 2 describes the physical properties of the materials constituting hTERCP.

$$\varepsilon_{WB} = \frac{T_{cwr} - T_{cws}}{T_h - T_{cws}} \tag{1}$$

Table 1. Range of design factors for hTERCP simulation model.

Symbol	Description	Minimum	Mid-Value	Maximum
T_{cws}	Temperature of cooling water supply	24 °C	26 °C	28 °C
$\dot{m}_w$	Flow rate of cooling water supply	0.014 kg/s		0.025 kg/s
ε_{WB}	Heat exchange effectiveness of water block	0.035		0.92
A_c	Heat exchange area of cooling surface	0.0256 m^2		0.036204 m^2
R_h	Thermal resistance of hot side	0.15 K/W		0.275 K/W

Table 2. Physical properties of the materials constituting hTERCP.

Material	Thermal Conductivity	Dimension	Thickness
Aluminum panel	237 W/m·K	400 mm × 400 mm	3 mm
Water block	237 W/m·K	80 mm × 40 mm	10 mm
Insulation	0.034 W/m·K	400 mm × 400 mm	9 mm
Thermoelectric module	Equation (7)	40 mm × 40 mm	4.7 mm

3.2. Thermoelectric Module Model

The Seebeck coefficient (α), electrical resistivity (ρ), and heat conductivity (κ), which are the thermophysical properties of n-type and p-type semiconductors, were calculated using Equations (2)–(4) based on the existing gray-box TEM model. The factors in these equations are based on the technical specifications of the TEM (Table 3). The maximum cooling capacity of TEM ($\dot{Q}_{c,max}$); maximum temperature difference between the hot and cold sides of the TEM (ΔT_{max}); number of thermoelement couples (N); maximum input current of TEM (I_{max}); area of TEM (A); and thickness of TEM (l) were obtained from

the technical data sheet for TEC1-12715 [31]. Based on the variables calculated from Equations (2)–(4), the lumped TEM properties can be derived using Equations (5)–(7).

$$\alpha = \frac{\dot{Q}_{c,max}(T_h - \Delta T_{max})}{N T_h^2 I_{max}} \tag{2}$$

$$]\rho = \frac{A f_p (T_h - \Delta T_{max})^2}{2 T_h l} \frac{\dot{Q}_{c,max}}{N^2 I_{max}^2} \tag{3}$$

$$\kappa = \frac{l(T_h - \Delta T_{max})^2}{A f_p T_h^2} \frac{\dot{Q}_{c,max}}{\Delta T_{max}} \tag{4}$$

$$S = 2\alpha N \tag{5}$$

$$R =]\rho \frac{4 N^2 l}{A f_p} \tag{6}$$

$$K = \kappa \frac{A f_p}{l} \tag{7}$$

Table 3. Technical specifications of the TEM.

Symbol	Description	Value
A	Dimension	40 mm × 40 mm
l	Thickness	4.7 mm
N	Number of thermoelement couples	127
ΔT_{max}	Maximum temperature difference	70 °C
V_{max}	Maximum input voltage	16 V
I_{max}	Maximum input current (DC)	15 A
$\dot{Q}_{c,max}$	Maximum cooling capacity	150.2 W
R	Electrical resistance (AC)	0.72–0.88 Ω

In the simulation, the cold-side temperature of the TEM (T_c) was set as 16 °C, which is the general design surface temperature of the radiant cooling panel to prevent condensation on the panel. It is approximately 1 °C higher than the dew point temperature of the conditioned zone at 25 °C dry-bulb temperature and 50% relative humidity. The hot-side temperature of TEM (T_h) and input current of TEM (I) were unknown factors determined using loop simulation for logical decision. The heating and cooling capacities of the TEMs ($\dot{Q}_h$, $\dot{Q}_c$) were calculated using Equations (8) and (9) and Equations (2)–(7) [32]. The total heat rejection from the TEM to the cooling water is equal to the heating capacity of the TEM, which can be calculated using Equation (10). The power consumption of the TEM was calculated using Equation (11).

$$\dot{Q}_h = SIT_h + \frac{1}{2}I^2 R - K(T_h - T_c) \tag{8}$$

$$\dot{Q}_c = SIT_h + \frac{1}{2}I^2 R - K(T_h - T_c) \tag{9}$$

$$\dot{Q}_{h,w} = \dot{m}_w C_{p,w}(T_{cwr} - T_{cws}) \tag{10}$$

$$P = I^2 R + SI(T_h - T_c) \tag{11}$$

3.3. Heat Transfer Model

Figure 4a shows the heat transfer from the hot side of the TEM to the cooling water. Heat conduction occurred through the water block from the hot side of the TEM. The heating capacity of hTERCP ($\dot{Q}_h$) was derived using Equation (12). As previously mentioned,

the thermal resistance of the hot side (R_h) was assumed based on a previous study, and the heat exchange area of the heating surface (A_h) was the same as that of the cooling surface. Figure 4b shows the heat transfer from the room to the cold side of the TEM. Radiative and convective heat transfer occurs through the aluminum panel from the room, and conductive heat transfer occurs from the aluminum panel to the cold side of the TEM. The cooling capacity of the hTERCP by radiation ($\dot{Q}_{c,rad}$) was calculated using Stefan–Boltzmann's law (Equation (13)), and the cooling capacity by convection ($\dot{Q}_{c,conv}$) was calculated using Equation (14).
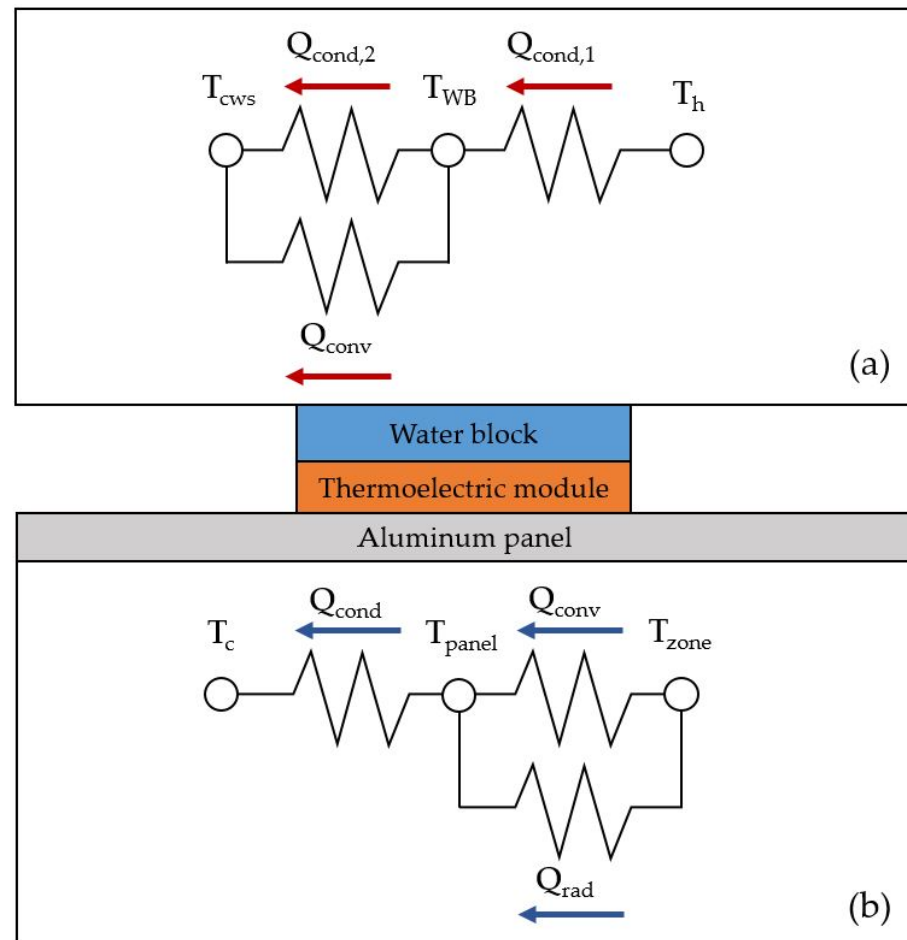

Figure 4. (**a**) Heat flows in the hot side of hTERCP. (**b**) Heat flows in the cold side of hTERCP.

The Stefan–Boltzmann constant (σ, 5.67×10^{-8} W/m^2/K^4) is a well-known factor, and the effective area of hTERCP (A) was set as 0.16 m $\times$ 0.16 m to bring the temperature difference between the hottest and coldest spots of the aluminum panel within 3 $^{\circ}$C based on the previous study [25]. The mean radiant temperature was assumed to be equal to the temperature of the conditioned zone, and the average surface temperature of the panel (T_s) was set to 1 $^{\circ}$C higher than the temperature of the coldest spot on the panel according to existing research [33]. The surface absorptivity of the cooling panel (ε, 0.97) and the convective heat transfer coefficients between the conditioned zone and cooling panel (h, 9.26 W/m^2/K) were determined as described in Chapter 26 of the *ASHRAE Handbook—Fundamentals* [34]. The total cooling capacity of the hTERCP was derived using Equation (15), and the power consumption of the hTERCP was calculated using Equation (16).

$$\dot{Q}_h = \frac{A_h}{R_h}(T_h - T_{cws}) \tag{12}$$

$$\dot{Q}_{c,rad} = \sigma A \varepsilon \left(MRT^4 - T_s^4 \right) \tag{13}$$

$$\dot{Q}_{c,conv} = h A (T_{zone} - T_s) \tag{14}$$

$$\dot{Q}_c = \dot{Q}_{c,rad} + \dot{Q}_{c,conv} \tag{15}$$

$$P = \dot{Q}_h - \dot{Q}_c \tag{16}$$

3.4. Loop Simulation

The cold-side temperature of the TEM (T_c) was determined based on the *ASHRAE* guidelines. The hot side temperature of TEM (T_h) and the input current of TEM (I) are unknown factors, and they can be derived using loop simulation by considering the heat balance between the TEM model and heat transfer model of hTERCP, as shown in Figure 5. In the first step, the hot-side temperature of the TEM was assumed to be the ambient temperature of the hot side ($T_{h,amb}$), which was analogous to the temperature of the cooling water supply. The input current of the TEM was assumed to be the ambient input current referred to in a previous experimental study [35]. Then, the heating capacities of the TEM and hTERCP were calculated using the TEM and heat transfer models of the hTERCP based on the assumed factors. If the absolute difference between the heating capacities of the TEM and the panel was within 1%, we would proceed to the next stage. However, if is the difference was greater than 1%, we would move to the previous stage to finely adjust the hot side temperature of the TEM. After adjusting the heating capacity, the input current of the TEM was adjusted to match the cooling capacity in the same way as calculating the heating capacity. Through the repeated calculations, the heating and cooling capacities of the TEM and hTERCP were derived, and the unknown factors, such as the hot-side temperature of the TEM and the input current of the TEM, were determined using loop simulation.
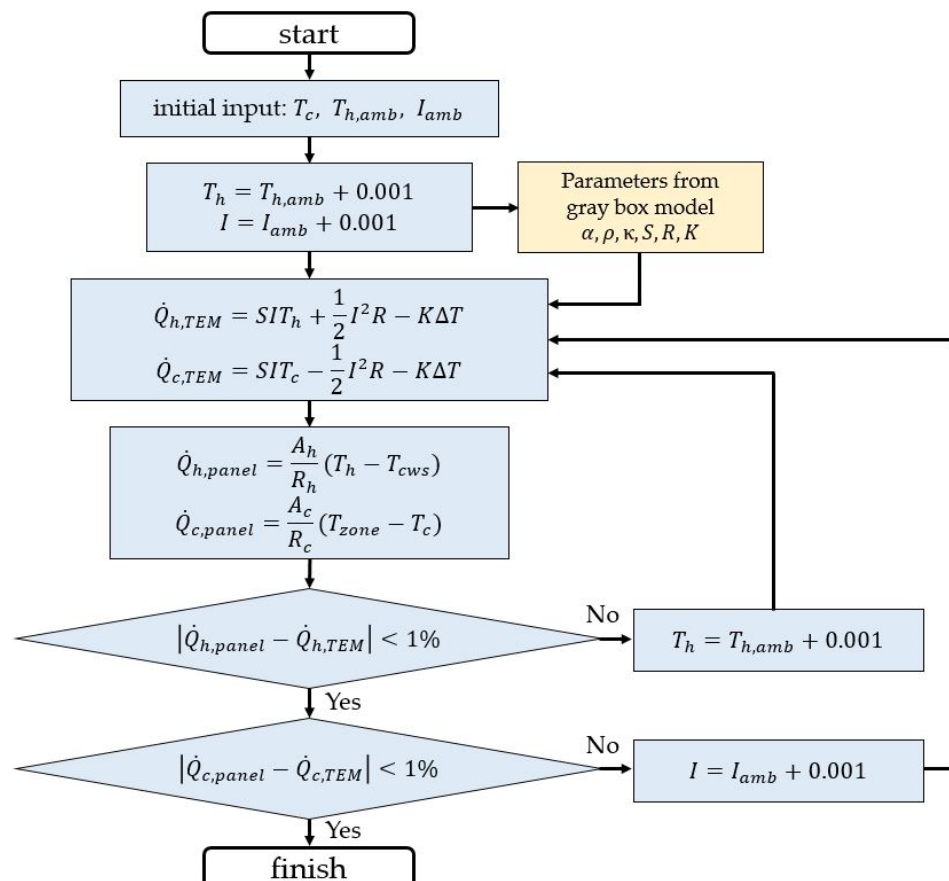

Figure 5. Simulation algorithm to derive the unknown factors.

3.5. Simulation Results

Table 4 presents the results of all simulation cases. The input parameters were the minimum and maximum values of the temperatures of the cooling water supply (T_{cws}), the flow rate of the cooling water supply ($\dot{m}_w$), the heat exchange effectiveness of the water block (ε_{WB}), the heat exchange area of the cooling surface (A_c), and the thermal resistance of the hot side (R_h). The output values were the cooling capacities of the hTERCP per unit area ($\dot{q}_c$), the power consumption of the hTERCP (P), and the coefficient of performance for the hTERCP (COP_{panel}).

Table 4. Results of all simulation cases.

	T_{cws} [°C]	$\dot{m}_w$ [kg/s]	ε_{WB} [-]	A_c [m^2]	R_h [K/W]	T_{cwr} [°C]	T_h [°C]	$\dot{q}_c$ [W/m^2]	P [W/m^2]	COP_{panel} [-]
Case 1	24	0.025	0.035	0.0256	0.275	24.05	25.4	136.55	51.94	2.629
Case 2	24	0.025	0.92	0.0256	0.275	24.05	25.4	136.55	45.14	3.025
Case 3	24	0.025	0.035	0.036204	0.275	24.05	25.4	136.55	36.73	3.718
Case 4	24	0.025	0.035	0.0256	0.15	24.05	25.4	136.55	51.54	2.649
Case 5	24	0.014	0.035	0.0256	0.275	24.08	25.4	136.55	57.26	2.385
Case 6	24	0.014	0.92	0.0256	0.275	24.08	25.4	136.55	51.15	2.67
Case 7	24	0.014	0.035	0.036204	0.275	24.08	25.4	136.55	40.49	3.372
Case 8	24	0.014	0.035	0.0256	0.15	24.08	25.4	136.55	51.54	2.649
Case 9	26	0.025	0.035	0.0256	0.275	26.04	27.6	136.55	75.66	1.805
Case 10	26	0.025	0.92	0.0256	0.275	26.04	27.6	136.55	66.06	2.067
Case 11	26	0.025	0.035	0.036204	0.275	26.04	27.6	136.55	53.5	2.552
Case 12	26	0.025	0.035	0.0256	0.15	26.04	27.6	136.55	74.93	1.822
Case 13	26	0.014	0.035	0.0256	0.275	26.09	27.6	136.55	82.99	1.645
Case 14	26	0.014	0.92	0.0256	0.275	26.09	27.6	136.55	66.52	2.053
Case 15	26	0.014	0.035	0.036204	0.275	26.09	27.6	136.55	58.68	2.327
Case 16	26	0.014	0.035	0.0256	0.15	26.09	27.6	136.55	74.93	1.822
Case 17	28	0.025	0.035	0.0256	0.275	28.06	29.8	136.55	104.87	1.302
Case 18	28	0.025	0.92	0.0256	0.275	28.06	29.8	136.55	91.82	1.487
Case 19	28	0.025	0.035	0.036204	0.275	28.06	29.8	136.55	74.16	1.841
Case 20	28	0.025	0.035	0.0256	0.15	28.06	29.8	136.55	104.17	1.311
Case 21	28	0.014	0.035	0.0256	0.275	28.11	29.8	136.55	115.28	1.185
Case 22	28	0.014	0.92	0.0256	0.275	28.11	29.8	136.55	92.37	1.478
Case 23	28	0.014	0.035	0.036204	0.275	28.11	29.8	136.55	81.51	1.675
Case 24	28	0.014	0.035	0.0256	0.15	28.11	29.8	136.55	104.17	1.311

The COP for the panel can be calculated using Equation (17), and the COPs of all the simulation cases were compared and analyzed. Cases 1, 5, 9, 13, 17, and 21 were the primary reference cases that were controlled by the temperature and flow rate of the cooling water to analyze the impact of the heat exchange effectiveness of the water block, the heat exchange areas of the cooling surface, and the thermal resistances of the hot side. These cases were selected as the primary references for the simulation because the temperature and flow rate of the cooling water are the operating parameters that can be controlled by the occupants after installing the equipment. Furthermore, these are design factors that can be used to validate the impact on the cooling performance of the hTERCP. Based on the analyzed data, the cooling performance prediction model equation was derived using an analysis of variance (ANOVA), as shown in Equation (18). Figure 6 verifies the simulation results by comparing the actual and predicted values obtained from the simulation model.

$$COP_{panel} = \frac{\dot{q}_c}{P} \tag{17}$$

$$P = \left(0.7124T_{cws} + 21.38924\dot{m}_w - 0.727482\varepsilon_{WB} - 133.93255A_c + 1.96821R_h - 7.10002\right)^2 \tag{18}$$
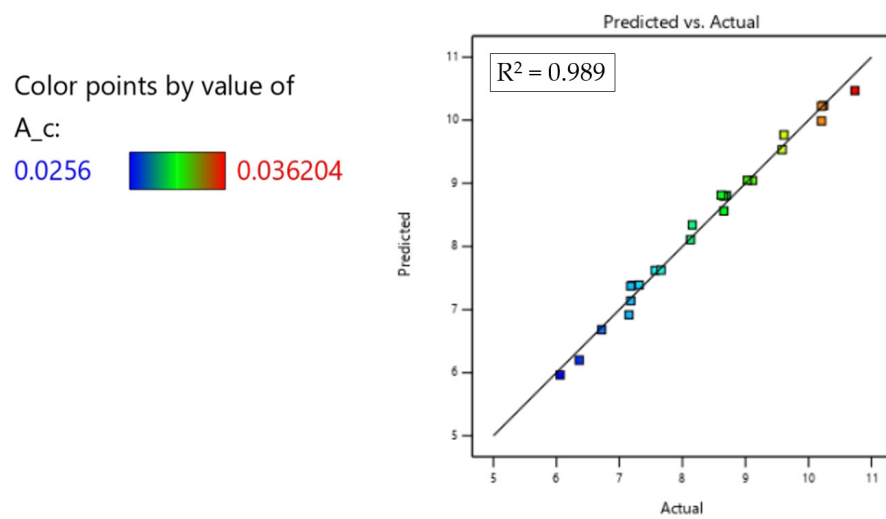
Figure 6. Comparison between the actual values and the predicted values by the simulation model.

4. Experimental Validation

4.1. Experiment Overview

A mockup model of the hTERCP was constructed to measure the power consumption and cooling capacity under various operating conditions, as shown in Figure 7. Four TEMs were attached to the aluminum panel, and four water blocks were installed on the hot side of each TEM. The TEMs between the aluminum panel and water blocks were fastened using bolts and nuts with thermal pastes to minimize contact resistance and improve thermal conductivity. The TEMs were arranged with intervals of 0.16 m in a square shape to ensure an acceptable temperature difference between the hottest and coldest spots of the panel during the cooling operation [35]. The effective area of the cooling panel was configured as a quarter of each TEM, and the cooling performance of one TEM was analyzed. Furthermore, a switched-mode power supply, which can independently control the direct current and voltage, was used to supply power to the TEMs. The performance specifications of the TEMs installed in the radiant cooling panels are listed in Table 2.

(a) Inside view   (b) Bottom view   (c) Top view
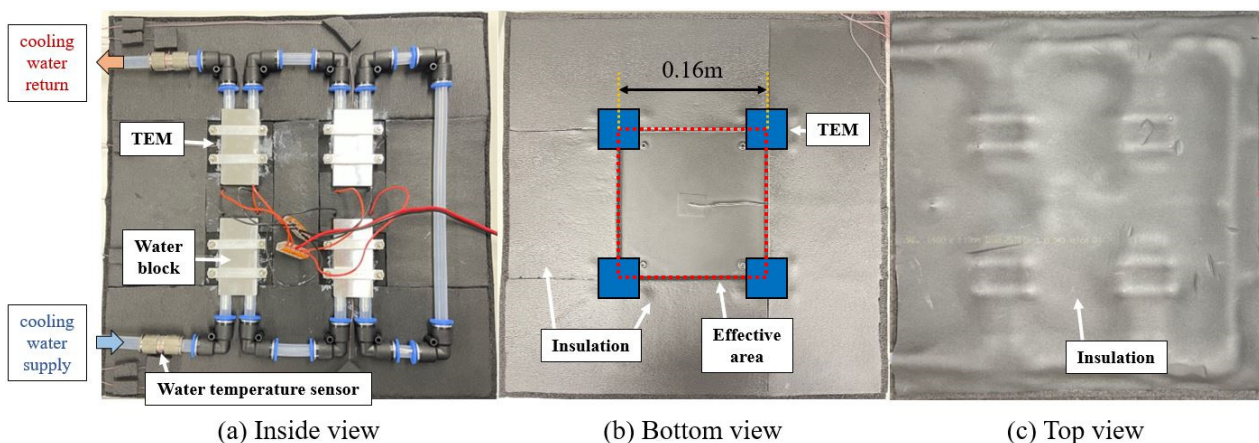
Figure 7. Mockup model of the hTERCP.

The aluminum panel had a square shape with a side of 0.4 m. The thickness of the radiant cooling panel was determined to be 3 mm considering the distortion from the mechanical bending stress. Rectangular water blocks were used as heat sinks to release heat from the hot side of the TEMs. The water blocks had a length of 80 mm and a width of 40 mm, which were larger than the TEMs, to cover the hot side spaciously. For water flow to the water blocks, ethylene-vinyl acetate copolymer tubes, which had flexibility

and sturdiness, were used as water pipes with external and internal diameters of 12 mm and 8 mm, respectively. The temperature of the supplied cooling water was replicated as the cooling water from a free cooling system that can be produced in Korean weather. The flow rate of the supply cooling water was classified as laminar flow or fully turbulent flow, depending on the shape of the water-cooling system using a variable-speed pump. Nitrile-butadiene rubber insulation, which has a thermal conductivity of 0.035 W/m·K and a thickness of 9 mm, was set up on the top side of the cooling panel to prevent undesirable heat transfer. Moreover, the surface of the cooling panel was painted in a matt black color to increase the absorptivity and improve the cooling performance by radiation.

The environmental chamber, which was set up at standard room temperature and humidity during the summer season according to the *ASHRAE* Standard 55 [36], was used to evaluate the cooling performance of the hTERCP. A cooling panel was installed at the top of the chamber as a ceiling panel. To measure the air temperature (T_{zone}), relative humidity (RH_{zone}), and MRT in the conditioned zone, smart probe sensors (Testo 605i) and a globe thermometer (Testo 605i) were set up inside the chamber, as shown in Figure 8.
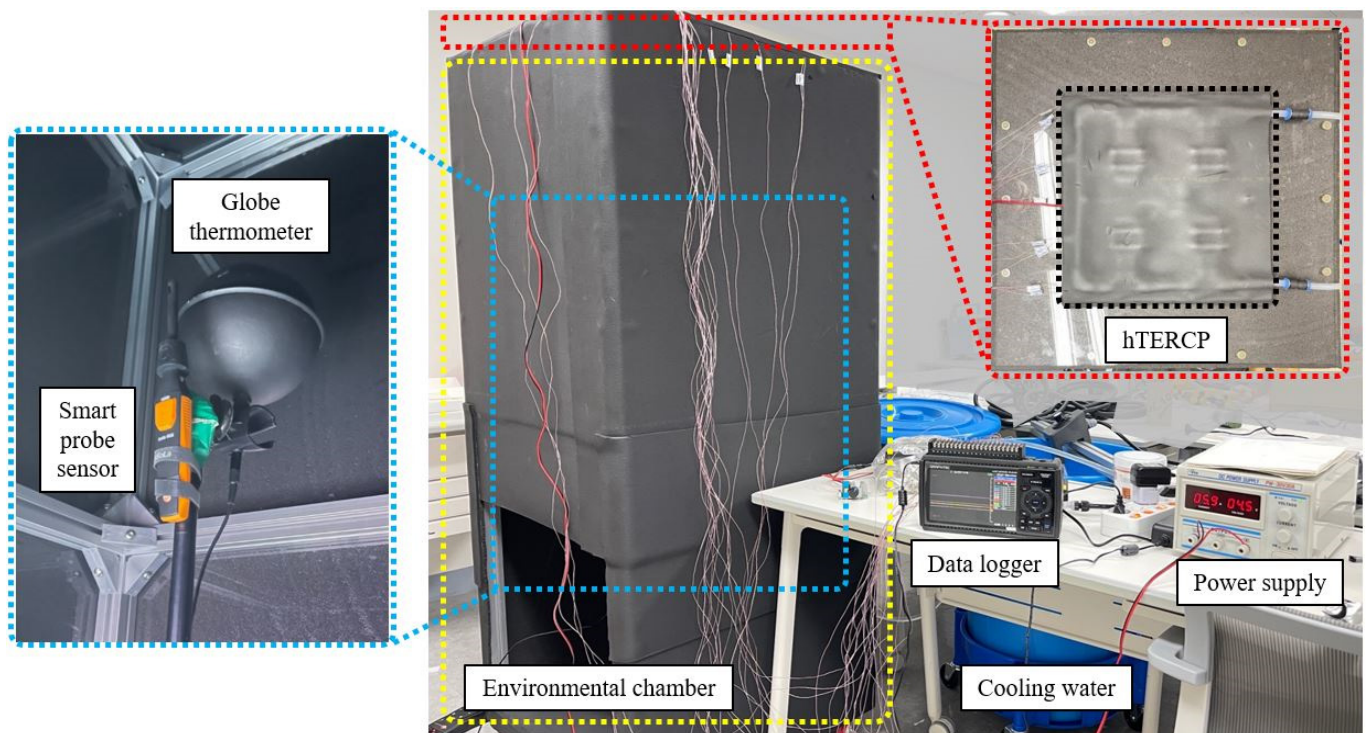

Figure 8. Configuration of the experiment for hTERCP.

During the experiments, the surface temperatures at nine points on the aluminum panel, the hot side and cold side temperatures of each TEM, and the water temperatures of the supply and return sides through the water blocks were measured using T-type thermocouples (TT-T-30-SLE, Omega Engineering, Norwalk, CT, USA, Error rate ± 0.5 °C). The data were recorded using a data logger (midi LOGGER GL840, GRAPGTEC, Yokohama, Japan, measuring range −200 to 400 °C, accuracy ± 0.5 °C). The thermocouples for the aluminum panel were uniformly located at the bottom surface to calculate the average temperature of the cooling surface (T_s). The thermocouples for the TEMs were installed between the aluminum panel and the cold side and between the water block and the hot side, as shown in Figure 9. To measure the water temperature, thermocouples were attached to the inlet and outlet water pipelines, which were made of copper. The data were recorded for at least 6000 s or longer with a 1 s resolution to measure various temperatures in the saturated condition.
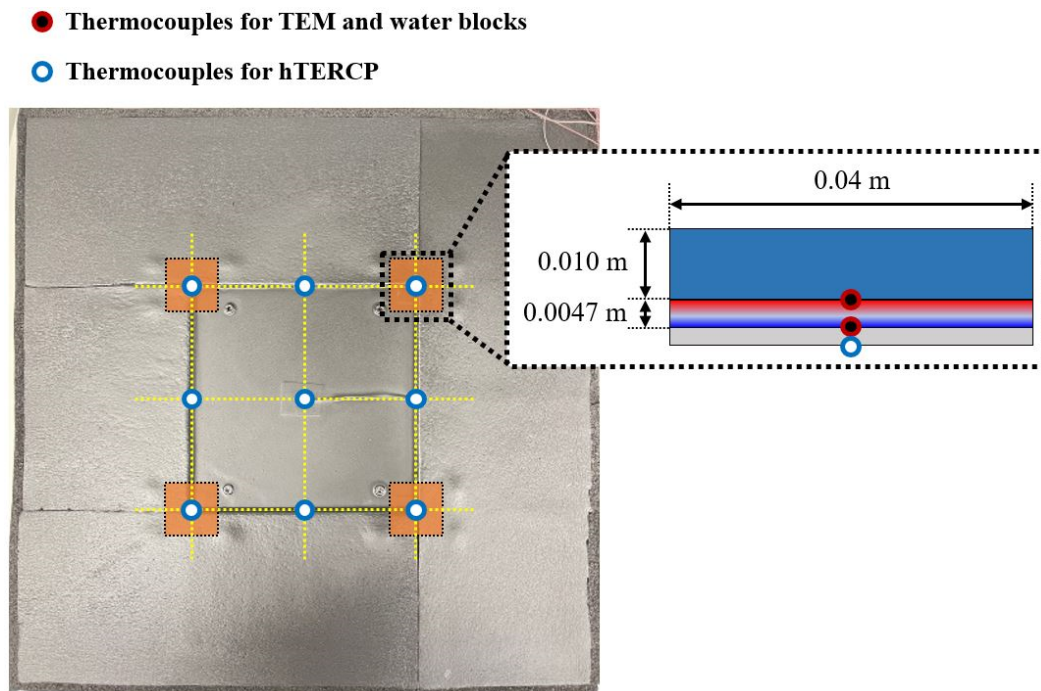
Figure 9. Measurement points of temperature for hTERCP by thermocouples.

4.2. Experimental Cases

A regular two-level factorial design was used in the experiments to validate the simulation models. The standard two-level factorial design method helps reduce the number of experiments according to the combinations of minimum and maximum factors of each independent variable. The independent and dependent variables should satisfy a linear relationship using this method.

The main operation-independent parameters were selected based on the temperatures of the supplied cooling water (T_{cws}), which can be produced from a free cooling system, and the cooling water flow rates ($\dot{m}_w$), which were classified by the fluid states. The range of the operating parameters was determined based on international standards and previous studies. The temperatures of the cooling water were adjusted by the chiller and heater with a constant temperature water tank, and they ranged from 24 to 28 °C, which can be produced from a cooling tower without the operation of the chiller, which is known as a free cooling system [29]. The cooling water flow rates can be easily controlled using a variable-speed pump with a dial controller. The two flow rates used in this experiment were 0.025 kg/s, in which the fluid state was fully turbulent, and 0.014 kg/s, which was a laminar state, according to the shape of the plumbing system. These values were calculated using theoretical equations [37,38], and the ranges of each parameter are presented in Table 5. The temperature and relative humidity of the conditioned zone (T_{zone}, RH_{zone}) were set to 25 °C and 50%, respectively, which are standard indoor conditions during the summer season based on the *ASHRAE* Standard 55 [36]. Eventually, six experimental cases were deduced, as shown in Table 6.

Table 5. Range of design factors for the hTERCP experiment.

Symbol	Description	Minimum		Maximum
T_{cws}	Temperature of cooling water supply	24 °C	26 °C	28 °C
$\dot{m}_w$	Flow rate of cooling water supply	0.014 kg/s		0.025 kg/s

Table 6. Experimental cases.

	T_{cws}	$\dot{m}_w$
Case 1	24 °C	0.025 kg/s
Case 2	24 °C	0.014 kg/s
Case 3	26 °C	0.025 kg/s
Case 4	26 °C	0.014 kg/s
Case 5	28 °C	0.025 kg/s
Case 6	28 °C	0.014 kg/s

4.3. Validation Methods and Results

4.3.1. Validation Methods

The measured data of the six experimental cases were used to validate the simulation models for the cooling capacity ($\dot{Q}_c$) and power consumption (*P*) of the hTERCP. The cooling capacity of the panel for radiation per effective area ($\dot{q}_{c,rad}$) was calculated in W/m^2 based on the average panel surface temperatures (T_s) measured by the thermocouples and MRT using a globe thermometer, as shown in Equation (19). Similarly, the cooling capacity of the panel for convection per effective area ($\dot{q}_{c,conv}$) was calculated using the surface heat transfer coefficient (*h*), average panel surface temperature (T_s), and conditioned zone air temperature (T_{zone}) from the smart probe sensor, as shown in Equation (20). The heat transfer coefficient of the cooling surface was assumed in accordance with the *ASHRAE* guidelines [39]. As shown in Equation (21), the total cooling capacity of the hTERCP per effective area ($\dot{q}_c$) is a combination of the radiative and convective heat transfer.

$$\dot{q}_{c,rad} = \sigma A \varepsilon \left(MRT^4 - T_s^4 \right) / A \tag{19}$$

$$\dot{q}_{c,conv} = h A (T_{zone} - T_s) / A \tag{20}$$

$$\dot{q}_c = \dot{q}_{c,rad} + \dot{q}_{c,conv} \tag{21}$$

The power consumption of the hTERCP (*P*) can be directly monitored using a switched-mode power supply. However, a quarter of the power consumption that can be monitored by the power supply should be considered when analyzing one TEM at the effective area from the power consumption of the four TEMs.

4.3.2. Validation Results

Table 7 lists the cooling capacities and power consumptions of the hTERCP per unit area derived from the experiment. The simulation results showed that the lower the cooling water temperature, the better the heat removal from the hot side of the TEM and the more effective the power consumption. Likewise, the flow rate of the cooling water had a relatively smaller effect on the cooling performance of the hTERCP compared with the temperature of the cooling water. As shown in Table 8, the cooling capacities and power consumptions calculated by the simulation model and experiment were comparatively analyzed by COP using Equation (17). Although there were some differences in the composition, the overall tendencies between the simulation and the experiment were similar.

Table 7. Cooling capacities and power consumptions per unit area from the experiment.

	T_{cws}	$\dot{m}_w$	T_{cwr}	T_c	T_h	$\dot{q}_c$	P
Case 1	24.1 °C	0.025 kg/s	24.4 °C	15.9 °C	25.3 °C	130 W/m^2	38.5 W/m^2
Case 2	23.9 °C	0.014 kg/s	24.4 °C	15.9 °C	25.3 °C	123.3 W/m^2	39.3 W/m^2
Case 3	25.9 °C	0.025 kg/s	26.1 °C	16.1 °C	27.2 °C	125.2 W/m^2	62.6 W/m^2
Case 4	26 °C	0.014 kg/s	26.3 °C	15.8 °C	27.9 °C	126.7 W/m^2	60.2 W/m^2
Case 5	27.9 °C	0.025 kg/s	28 °C	16.1 °C	29.3 °C	121.6 W/m^2	79.3 W/m^2
Case 6	27.9 °C	0.014 kg/s	28.4 °C	16.2 °C	29.7 °C	120.9 W/m^2	78.1 W/m^2

Table 8. Comparison of COP between simulation and experiment results.

	Simulation COP					**Experiment COP**			
T_{cws}	$\dot{m}_w$	0.014 kg/s	0.025 kg/s	ΔCOP		T_{cws}	$\dot{m}_w$	0.014 kg/s	0.025 kg/s	ΔCOP
28 °C		1.185	1.302	+9.9%		28 °C		1.533	1.548	+1.0%
26 °C		1.645	1.805	+9.7%		26 °C		2.000	2.105	+5.2%
ΔCOP		+38.9%	+38.6%			ΔCOP		+30.4%	+36.0%	

	Simulation COP					**Experiment COP**			
T_{cws}	$\dot{m}_w$	0.014 kg/s	0.025 kg/s	ΔCOP		T_{cws}	$\dot{m}_w$	0.014 kg/s	0.025 kg/s	ΔCOP
26 °C		1.645	1.805	+9.7%		26 °C		2.000	2.105	+5.2%
24 °C		2.385	2.629	+10.2%		24 °C		3.129	3.377	+7.9%
ΔCOP		+44.9%	+45.7%			ΔCOP		+56.5%	+60.4%	

4.4. Uncertainty Analysis

Based on the *ASHRAE* guidelines [40] and previous studies [41], an uncertainty analysis of the measured parameters was conducted to validate the experiments. As shown in Equation (22), the overall uncertainty for the measured values (U_y) consists of two errors: propagation error (B_y) and random error (P_y). The propagation error (B_y) can be calculated using a fixed error (b_{xi}), which was obtained by multiplying the standard deviation of the measured temperature (S_r) and the sensor error of the thermocouples by Equation (23) in this study. The random error (P_y) can be defined by Equation (24) based on the standard deviation and mean value (M) of the measurements. The overall uncertainty of the experiments was derived using the measured parameters (x_i). The overall uncertainty values of the temperature and flow rate of cooling water for hTERCP were 0.18% and 0.70%, respectively.

$$U_y = \sqrt{\left(B_y^2 + P_y^2\right)} \tag{22}$$

$$B_y = \sqrt{\left[\sum_{i=1}^{n}\left(\frac{dy}{dx_i}B_{x_i}\right)^2\right]} \tag{23}$$

$$P_y = \frac{2S_r}{\sqrt{M}} \tag{24}$$

5. Discussion

A parametric analysis was conducted to derive the effects of the five design parameters. The temperature and flow rate of the cooling water, heat exchange effectiveness of the water block, heat exchange area of the cooling surface, and thermal resistance of the hot side were selected as design parameters to improve the cooling performance of the hTERCP, as described in Table 1. As derived in Section 3.5 and shown in Table 8, the temperature of the cooling water was found to have a significant effect of 38.6–45.7% on the cooling

performance, and the flow rate of the cooling water was confirmed to have a relatively little influence of 9.7–10.2% based on the simulation results.

As seen in Table 9, the heat exchange area of the cooling surface was analyzed to have a high influence of 41.4% on the cooling performance. On the other hand, the heat exchange effectiveness of the water block and heat resistance of the hot side had little effect on the cooling performance: 11.9–24.8% and 0.7–11.1%, respectively. In the case of the heat resistance of the hot side, almost no effect (0.7–1%) was found when the fluid was in a turbulent flow.

Table 9. Impact analysis of design parameters by comparison of COPs.

	T_{cws} [°C]	$\dot{m}_w$ [kg/s]	ε_{WB} [-]	A_c [m²]	R_h [K/W]	T_{cwr} [°C]	T_c [°C]	T_h [°C]	COP_{panel} [-]	ΔCOP
Case 1	24	0.025	0.035	0.0256	0.275	24.05	16	25.4	2.629	
Case 1-ε_{WB}	24	0.025	0.92	0.0256	0.275	24.05	16	25.4	3.025	+15.1%
Case 1-A_c	24	0.025	0.035	0.036204	0.275	24.05	16	25.4	3.718	+41.4%
Case 1-R_h	24	0.025	0.035	0.0256	0.15	24.05	16	25.4	2.649	+0.8%
Case 2	24	0.014	0.035	0.0256	0.275	24.08	16	25.4	2.385	
Case 2-ε_{WB}	24	0.014	0.92	0.0256	0.275	24.08	16	25.4	2.67	+11.9%
Case 2-A_c	24	0.014	0.035	0.036204	0.275	24.08	16	25.4	3.372	+41.4%
Case 2-R_h	24	0.014	0.035	0.0256	0.15	24.08	16	25.4	2.649	+11.1%
Case 3	26	0.025	0.035	0.0256	0.275	26.04	16	27.6	1.805	
Case 3-ε_{WB}	26	0.025	0.92	0.0256	0.275	26.04	16	27.6	2.067	+14.5%
Case 3-A_c	26	0.025	0.035	0.036204	0.275	26.04	16	27.6	2.552	+41.4%
Case 3-R_h	26	0.025	0.035	0.0256	0.15	26.04	16	27.6	1.822	+1%
Case 4	26	0.014	0.035	0.0256	0.275	26.09	16	27.6	1.645	
Case 4-ε_{WB}	26	0.014	0.92	0.0256	0.275	26.09	16	27.6	2.053	+24.8%
Case 4-A_c	26	0.014	0.035	0.036204	0.275	26.09	16	27.6	2.327	+41.4%
Case 4-R_h	26	0.014	0.035	0.0256	0.15	26.09	16	27.6	1.822	+10.8%
Case 5	28	0.025	0.035	0.0256	0.275	28.06	16	29.8	1.302	
Case 5-ε_{WB}	28	0.025	0.92	0.0256	0.275	28.06	16	29.8	1.487	+14.2%
Case 5-A_c	28	0.025	0.035	0.036204	0.275	28.06	16	29.8	1.841	+41.4%
Case 5-R_h	28	0.025	0.035	0.0256	0.15	28.06	16	29.8	1.311	+0.7%
Case 6	28	0.014	0.035	0.0256	0.275	28.11	16	29.8	1.185	
Case 6-ε_{WB}	28	0.014	0.92	0.0256	0.275	28.11	16	29.8	1.478	+24.8%
Case 6-A_c	28	0.014	0.035	0.036204	0.275	28.11	16	29.8	1.675	+41.4%
Case 6-R_h	28	0.014	0.035	0.0256	0.15	28.11	16	29.8	1.311	+10.7%

As a result of analyzing the influence of design variables on hTERCP energy performance, it was confirmed that the influence was large in the order of the temperature of the cooling water, the heat exchange area of the cooling surface, the heat exchange effectiveness of the water block, the flow rate of the cooling water, and the thermal resistance of the hot side. Based on the analyzed results, in order to improve the energy performance of hTERCP, it is effective to use the method introduced in Section 3.1 and improve it in the above order.

6. Conclusions

A cooling performance prediction model for the hTERCP was developed based on the simulation of the thermoelectric and heat transfer models with experimental validation. The simulation model was designed using five design factors: the temperature of the cooling water, the flow rate of the cooling water, the heat exchange area of the cooling surface, the heat exchange effectiveness of the water block, and the heat resistance of the hot side. The prediction model's coefficient of determination (R^2, R-squared) was 0.989, which was verified within a 15% error bound.

In order to verify the proposed simulation model, a mockup model of the hTERCP was constructed and tested in an environmental chamber. Four TEMs with water blocks were attached to the aluminum panel, and the effective area of the cooling panel was configured as a quarter of each TEM to analyze the cooling performance of one TEM. The cooling capacities and the power consumptions of the simulation model and experiment were comparatively analyzed by COP. Despite some differences in the composition, the overall trends between the simulation and the experiment were similar.

Consequently, the effects of the five design parameters were analyzed for the energy-saving potential of the hTERCP. The temperature of the cooling water and the heat exchange area of the cooling surface were found to have a significant effect of 38.6–45.7% and 41.4% on the cooling performance. On the other hand, the heat exchange effectiveness of the water block, the flow rate of the cooling water, and the thermal resistance of the hot side were confirmed to have relatively little influence: 11.9–24.8%, 9.7–10.2%, and 0.7–11.1%, respectively. Effectively improving the energy performance of hTERCP is possible in the above order using the method introduced in Section 3.1.

In this study, the hTERCP was set at a constant surface temperature of 16 °C to obtain the maximum cooling capacity. Radiant cooling panels generally control the cooling capacity based on the number of operating TEMs. The variable temperature, however, could be utilized in the hTERCP system to remove changeable sensible cooling loads using the fast response of the TEM. Therefore, further research could be conducted to control the surface temperature to adjust the cooling performance and improve the models of hTERCP.

Author Contributions: Conceptualization, formal analysis, data curation, writing—original draft preparation: M.K.; investigation, methodology: Y.-K.K.; resources, validation: J.J.; writing—review and editing, visualization, supervision: J.-W.J. All authors have read and agreed to the published version of the manuscript.

Institutional Review Board Statement: Not applicable.

Informed Consent Statement: Not applicable.

Data Availability Statement: Not applicable.

Conflicts of Interest: The authors declare no conflict of interest.

References

1. Zuazua-Ros, A.; Martín-Gómez, C.; Ibañez-Puy, E.; Vidaurre-Arbizu, M.; Gelbstein, Y. Investigation of the Thermoelectric Potential for Heating, Cooling and Ventilation in Buildings: Characterization Options and Applications. *Renew. Energy* **2019**, *131*, 229–239. [CrossRef]
2. Luo, Y.; Zhang, L.; Liu, Z.; Yu, J.; Xu, X.; Su, X. Towards Net Zero Energy Building: The Application Potential and Adaptability of Photovoltaic-Thermoelectric-Battery Wall System. *Appl. Energy* **2020**, *258*, 114066. [CrossRef]
3. Shen, L.; Pu, X.; Sun, Y.; Chen, J. A Study on Thermoelectric Technology Application in Net Zero Energy Buildings. *Energy* **2016**, *113*, 9–24. [CrossRef]
4. Liu, Z.; Zhang, L.; Gong, G.; Li, H.; Tang, G. Review of Solar Thermoelectric Cooling Technologies for Use in Zero Energy Buildings. *Energy Build.* **2015**, *102*, 207–216. [CrossRef]
5. Lim, H.; Jeong, J.W. Energy Saving Potential of Thermoelectric Modules Integrated into Liquid Desiccant System for Solution Heating and Cooling. *Appl. Therm. Eng.* **2018**, *136*, 49–62. [CrossRef]
6. Zhang, X.; Huang, Y.; Chen, Z. A Hybrid System Integrating Photovoltaic Module and Thermoelectric Devices for Power and Cooling Cogeneration. *Sol. Energy* **2022**, *239*, 350–358. [CrossRef]
7. Ibañez-Puy, M.; Bermejo-Busto, J.; Martín-Gómez, C.; Vidaurre-Arbizu, M.; Sacristán-Fernández, J.A. Thermoelectric Cooling Heating Unit Performance under Real Conditions. *Appl. Energy* **2017**, *200*, 303–314. [CrossRef]
8. Sarbu, I.; Dorca, A. A Comprehensive Review of Solar Thermoelectric Cooling Systems. *Int. J. Energy Res.* **2018**, *42*, 395–415. [CrossRef]
9. Cai, Y.; Wang, W.W.; Liu, C.W.; Ding, W.T.; Liu, D.; Zhao, F.Y. Performance Evaluation of a Thermoelectric Ventilation System Driven by the Concentrated Photovoltaic Thermoelectric Generators for Green Building Operations. *Renew. Energy* **2020**, *147*, 1565–1583. [CrossRef]

10. Vián, J.G.; Astrain, D.; Domínguez, M. Numerical Modelling and a Design of a Thermoelectric Dehumidifier. *Appl. Therm. Eng.* **2002**, *22*, 407–422. [CrossRef]
11. Luo, Y.; Zhang, L.; Liu, Z.; Wu, J.; Zhang, Y.; Wu, Z. Three Dimensional Temperature Field of Thermoelectric Radiant Panel System: Analytical Modeling and Experimental Validation. *Int. J. Heat Mass Transf.* **2017**, *114*, 169–186. [CrossRef]
12. Heremans, J.P.; Jovovic, V.; Toberer, E.S.; Saramat, A.; Kurosaki, K.; Charoenphakdee, A.; Yamanaka, S.; Snyder, G.J. Enhancement of Thermoelectric of the Electronic Density of States. *Science* **2008**, *321*, 1457–1461. [CrossRef]
13. Byrnes, J.; Mitchell, D.R.G.; Aminorroaya Yamini, S. Thermoelectric Performance of Thermally Aged Nanostructured Bulk Materials—A Case Study of Lead Chalcogenides. *Mater. Today Phys.* **2020**, *13*, 100190. [CrossRef]
14. Androulakis, J.; Lin, C.H.; Kong, H.J.; Uher, C.; Wu, C.I.; Hogan, T.; Cook, B.A.; Caillat, T.; Paraskevopoulos, K.M.; Kanatzidis, M.G. Spinodal Decomposition and Nucleation and Growth as a Means to Bulk Nanostructured Thermoelectrics: Enhanced Performance in $Pb_{1-x}Sn_xTe$-PbS. *J. Am. Chem. Soc.* **2007**, *129*, 9780–9788. [CrossRef]
15. Shoeibi, S.; Kargarsharifabad, H.; Sadi, M.; Arabkoohsar, A.; Mirjalily, S.A.A. A Review on Using Thermoelectric Cooling, Heating, and Electricity Generators in Solar Energy Applications. *Sustain. Energy Technol. Assess.* **2022**, *52*, 102105. [CrossRef]
16. Irshad, K.; Habib, K.; Algarni, S.; Saha, B.B.; Jamil, B. Sizing and Life-Cycle Assessment of Building Integrated Thermoelectric Air Cooling and Photovoltaic Wall System. *Appl. Therm. Eng.* **2019**, *154*, 302–314. [CrossRef]
17. Cheon, S.Y.; Lim, H.; Jeong, J.W. Applicability of Thermoelectric Heat Pump in a Dedicated Outdoor Air System. *Energy* **2019**, *173*, 244–262. [CrossRef]
18. Lertsatitthanakorn, C.; Wiset, L.; Atthajariyakul, S. Evaluation of the Thermal Comfort of a Thermoelectric Ceiling Cooling Panel (TE-CCP) System. *J. Electron. Mater.* **2009**, *38*, 1472–1477. [CrossRef]
19. Lertsatitthanakorn, C.; Tipsaenprom, W.; Srisuwan, W.; Atthajariyakul, S. Study on the Cooling Performance and Thermal Comfort of a Thermoelectric Ceiling Cooling Panel System. *Indoor Built Environ.* **2008**, *17*, 525–534. [CrossRef]
20. Lim, H.; Jeong, J.W. Energy Saving Potential of Thermoelectric Radiant Cooling Panels with a Dedicated Outdoor Air System. *Energy Build.* **2018**, *169*, 353–365. [CrossRef]
21. Luo, Y.; Zhang, L.; Liu, Z.; Wu, J.; Zhang, Y.; Wu, Z. Numerical Evaluation on Energy Saving Potential of a Solar Photovoltaic Thermoelectric Radiant Wall System in Cooling Dominant Climates. *Energy* **2018**, *142*, 384–399. [CrossRef]
22. Shen, L.; Tu, Z.; Hu, Q.; Tao, C.; Chen, H. The Optimization Design and Parametric Study of Thermoelectric Radiant Cooling and Heating Panel. *Appl. Therm. Eng.* **2017**, *112*, 688–697. [CrossRef]
23. Shen, L.; Xiao, F.; Chen, H.; Wang, S. Investigation of a Novel Thermoelectric Radiant Air-Conditioning System. *Energy Build.* **2013**, *59*, 123–132. [CrossRef]
24. Lim, H.; Kang, Y.K.; Jeong, J.W. Development of Empirical Models to Predict Cooling Performance of a Thermoelectric Radiant Panel. *Energy Build.* **2019**, *202*, 109387. [CrossRef]
25. Lim, H.; Kang, Y.K.; Jeong, J.W. Thermoelectric Radiant Cooling Panel Design: Numerical Simulation and Experimental Validation. *Appl. Therm. Eng.* **2018**, *144*, 248–261. [CrossRef]
26. Lim, H.; Jeong, J.W. Numerical and Experimental Study on the Performance of Thermoelectric Radiant Panel for Space Heating. *Materials* **2020**, *13*, 550. [CrossRef]
27. Lim, H.; Kang, Y.K.; Jeong, J.W. Application of a Phase Change Material to a Thermoelectric Ceiling Radiant Cooling Panel as a Heat Storage Layer. *J. Build. Eng.* **2020**, *32*, 101787. [CrossRef]
28. The American Society of Heating, Refrigeration and Air Conditioning Engineers (ASHRAE). *ASHRAE Handbook: HVAC Systems and Equipment, Chapter 6: Radiant Heating and Cooling*; ASHRAE: Atlanta, GA, USA, 2016.
29. Ha, J.-W.; Kim, Y.-J.; Kim, H.-Y.; Song, Y.-H. Verification of Low-temperature Condenser Water and Operation Time considering Climate Zones. *J. Korean Inst. Archit. Sustain. Environ. Build. Syst.* **2020**, *14*, 298–309. [CrossRef]
30. Hahm, H.C.; Park, C.Y. Experimental Study on the Performance of an Electric Component Liquid Cooling System with Variation of the Waterblock Internal Shape. *Korean J. Air-Cond. Refrig. Eng.* **2013**, *25*, 331–337. [CrossRef]
31. TEC1-12715, Specification of Thermoelectric Module, High Performance and Highly Reliable Solution for Cooling and Heating Applications. Available online: https://datasheetspdf.com/pdf/869807/Creativetechnology/TEC1-12715/1 (accessed on 5 November 2022).
32. Chen, M.; Snyder, G.J. Analytical and Numerical Parameter Extraction for Compact Modeling of Thermoelectric Coolers. *Int. J. Heat Mass Transf.* **2013**, *60*, 689–699. [CrossRef]
33. Jeong, J.-W.; Mumma, S. Designing a Dedicated Outdoor Air System with Ceiling Radiant Cooling Panels. *ASHRAE J.* **2006**, *48*, 56–66.
34. The American Society of Heating, Refrigeration and Air Conditioning Engineers (ASHRAE). *ASHRAE Handbook-Fundamentals, Chapter 26: Heat, Air, and Moisture Control in Building Assemblies—Material Roperties*; ASHRAE: Atlanta, GA, USA, 2013.
35. Kim, M.; Cho, H.; Lee, S.; Joung, J.; Jeong, J. Experimental analysis and design of hydraulic thermoelectric radiant cooling panel. In Proceedings of the 42nd AIVC Conference Proceedings 2022, Rotterdam, The Netherlands, 5–6 October 2022; pp. 578–583.
36. *ASHRAE Standard 55*; Thermal Environmental Conditions for Human Occupancy. ASHRAE: Atlanta, GA, USA, 2010.
37. Churchill, S.W.; Ozoe, H. Correlations for laminar forced convection in flow over an isothermal flat plate and in developing and fully developed flow in an isothermal tube. *J. Heat Transf.* **1973**, *95*, 416–419. [CrossRef]
38. Thomas, W.C. Note on the heat transfer equation for forced convection flow over a flat plate with an unheated starting length. *Mech. Eng. News* **1977**, *9*, 361–368.

39. The American Society of Heating, Refrigeration and Air Conditioning Engineers (ASHRAE). *ASHRAE Handbook-Fundamentals, Chapter 4: Heat Transfer*; ASHRAE: Atlanta, GA, USA, 2013.

40. *ASHRAE Guideline 2-2010*; Engineering Analysis of Experimental Data. ASHRAE: Atlanta, GA, USA, 2010.

41. Lim, H.; Lee, S.J.; Su, Y.; Jeong, J.W. Experimental Study and Prediction Model of a Liquid Desiccant Unit for Humidification during the Heating Season. *J. Build. Eng.* **2022**, *45*, 103549. [CrossRef]